Research Article | Vol. 28, No. 8 / 13 April 2020 / Optics Express 12093
Optics EXPRESS

Femtosecond time-resolved pump-probe measurements on percolating gold in the ablation regime

G. DE HAAN,[1,2,*] J. HERNANDEZ-RUEDA,[1] AND P. C. M. PLANKEN[1,2]

[1]Advanced Research Center for Nanolithography (ARCNL), Science Park 110, 1098 XG Amsterdam, The Netherlands
[2]Van der Waals-Zeeman Institute, University of Amsterdam, Science Park 904, 1098 XH Amsterdam, The Netherlands
[*]g.dehaan@arcnl.nl

Abstract: We report on femtosecond laser ablation experiments on percolating gold layers deposited on a glass substrate. In our experiments, we measure changes in optical transmission and reflection induced by single, high-intensity infrared laser pulses as a function of the time delay between the pump and the probe. For the highest pump intensities we find that on a time scale of about 150 ps after excitation, the transmission and reflection approach values close to the substrate values. We attribute this rapid ablation to vaporization of the entire layer when the injected energy exceeds the cohesive energy of the material. This vaporization results in the rapid transformation of the gold layer into a sufficiently dilute mist of atoms and nano-particles which renders the material almost optically transparent to the probe pulse. SEM images of the surfaces show how the morphology of the films changes at relatively low excitation intensities and show the complete removal of the gold at high intensities. We find that the ablation threshold for percolating Au on glass is 2.3×10^{11} W/cm^2, which is two orders of magnitude lower than the damage threshold for continuous gold layers as reported in the literature.

1. Introduction

Discontinuous, nano-structured metallic surfaces exhibit different linear and nonlinear optical properties compared to continuous metallic layers [1–3]. Examples of enhanced nonlinear optical effects range from the generation of terahertz pulses [4–6] to strongly enhanced second harmonic generation [7,8]. An example of a nanostructured surface that has been widely studied is percolating gold. Gold is a non-oxidizing metal and its physical and linear optical properties are generally well understood [9,10]. When physical vapor deposition is used to make gold layers on glass, a nano-structured surface forms, consisting of isolated islands that coalesce into larger networks with increasing average layer thickness. When deposition continues, an average layer thickness is reached where connected networks of gold provide an uninterrupted conducting path for electrons from one end of the sample to the other. The threshold where this occurs is called the percolation threshold and depends on the type of substrate [11,12], but typically occurs around an average layer thickness of about 6 nm for gold on glass.

The linear and nonlinear optical properties of gold around the percolation threshold are reasonably well understood. However, little is known about the effects of percolation in the extreme nonlinear optical regime where laser pulse powers are high enough that damage and even ablation takes place. It is known, for example, that optical field strengths can be strongly enhanced in the gaps between the metal structures of a nanostructured metal surface such as percolating gold [13]. What is not known, is what the time-dependent response of such a surface is when the intensity reaches and exceeds the damage threshold.

#390509 https://doi.org/10.1364/OE.390509
Journal © 2020 Received 13 Feb 2020; revised 20 Mar 2020; accepted 30 Mar 2020; published 8 Apr 2020

Optics EXPRESS

Here, we show measurements of the transient optical response of a percolating gold surface after optical excitation with a strong 56 fs duration pump pulse, powerful enough to ablate material. In our experiments, a pump pulse excites the percolating gold and a time-delayed attenuated probe pulse measures the change in optical reflection and transmission induced by the excitation. Our results show that the measured pump-induced optical reflection change for a percolating gold surface initially shows a rapid, strong increase, followed by a slower decrease to negative values, with a rate that is fluence-dependent. For the highest pump fluences, the induced optical changes seem to saturate and are quasi-constant during the first two picoseconds. Transmission measurements show similar dynamics, with an initial sharp decrease in transmission, a quasi-constant plateau during the first two picoseconds, followed by a slower increase to positive values on longer time scales. For the highest intensities, the transmission and reflection of the samples approach the substrate values on a time scale of about 150 ps. We argue that this means that the percolating gold layer has become nearly optically transparent and suggests that it has changed into a relatively dilute "mist" of atoms and/or nanoparticles on this time scale. We attribute this to the percolating nature of the film which gives rise to significantly more absorption compared to a continuous gold layer, and to the small average thickness of the layer which makes vaporization of the entire layer on this time scale plausible. We find that the ablation threshold for percolating Au is 2.3×10^{11} W/cm^2, which is two orders of magnitude lower than the damage threshold for continuous gold layers reported in literature.

2. Experimental setup

A schematic drawing of the experimental setup is shown in Fig. 1. An amplified Ti:Sapphire laser (Coherent Astrella) with a repetition rate of 1 kHz, a central wavelength of 800 nm, a pulse length of 35 fs and a maximum pulse energy of 6 mJ is used. The laser pulses are sent into an optical parametric amplifier (OPA, HE-TOPAS from Light Conversion). The OPA generates infrared laser pulses and is tuned to a wavelength of 1300 nm with a pulse energy of about 1 mJ. A wavelength of 1300 nm is used because at this wavelength the OPA has a high output power and because we want to reduce the probability of directly exciting interband transitions, which are known to occur at wavelengths shorter than about 502 nm in Au [14]. A non-collinear autocorrelator is used to measure the pulse length. Assuming a Gaussian temporal profile, a pulse duration of 56 ± 5 fs for both the pump and the probe pulses is measured. Both pump and probe pulses are s-polarized.

The output of the OPA is split into a stronger pump beam and a weaker probe beam using a 90/10 beam splitter. The pump beam passes through a mechanical chopper which is synchronized with the 1 kHz pulse train from the laser. With a 50% duty-cycle, the chopper reduces the repetition rate of the pump to 500 Hz, so that every other pump pulse is blocked. Afterward, the beam reflects off a rapidly rotating galvo mirror which, when in the "on" position, directs the pump pulse through the setup and when in the "off" position, directs the pump into a beam dump. The galvo mirror is phase-locked to the chopper allowing us to select individual pulses to enter the setup. Selected pump pulses are sent through two wire-grid polarizers to attenuate the pulse energy. Finally, using a 10 cm focal length lens, the pump pulse is focused onto the sample to a spot size with a diameter of approximately 100 μm. The sample is mounted on a computer-controlled xy-translation stage to translate the sample in the plane parallel to the sample surface. Each pump pulse either removes or damages the Au layer locally. To ensure that every pump pulse illuminates an undamaged part of the sample, the sample-stage moves the sample 400 μm to a new position after each pump shot.

A weak, 180 nJ probe pulse, time-delayed by first sending it to a variable optical delay line, is focused onto the same spot on the sample under a 15-degree angle with respect to the pump beam. The diameter of the probe focal spot is approximately 50 μm, twice as small as the pump beam diameter. The transmission and reflection of the probe pulse are then measured

Optics EXPRESS

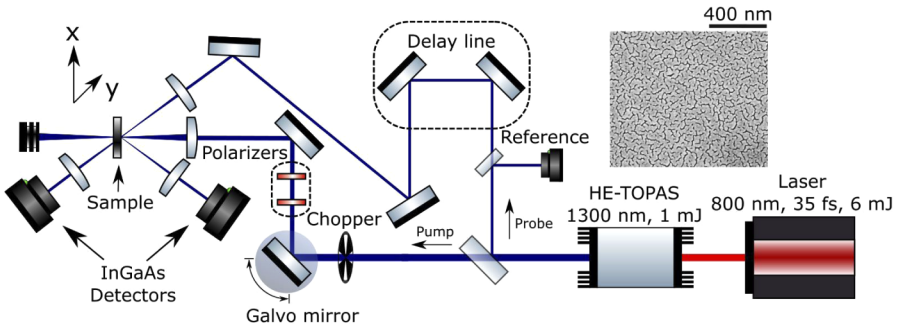

Fig. 1. Schematic drawing of the setup. The laser beam coming out of the HE-TOPAS, with a central wavelength of 1300 nm, is split into pump and probe. After this, the repetition rate of the pump is halved using a mechanical chopper. Using a phase-locked rapidly rotating galvo mirror we select single pump pulses. The power of these pulses can be attenuated using two wire grid polarizers. After a pump pulse is incident on the sample a time-delayed probe pulse is measured in both reflection and transmission using two InGaAs detectors. Using an automated xy-translation stage we move the sample to a new position after every pump pulse. The inset in the top right corner shows an SEM image of a typical percolating gold surface.

simultaneously using two InGaAs detectors. A third InGaAs detector is used to measure a reference beam that is split off from the probe. This reference is used to monitor fluctuations in the OPA output power. Since the repetition rate of the pump is half that of the probe, we measure the reflection/transmission of a probe pulse when the pump is blocked, and when the pump is transmitted, allowing us to measure the pump-induced transmission and reflection changes. After the reflection and transmission change are measured, the sample stage moves the sample to a new position. For each delay between pump and probe, this process is repeated 25 times to improve the signal-to-noise ratio of the measured probe transmission and reflection. Both the reflection and transmission changes are plotted normalized to the initial unperturbed reflection R_0 and transmission T_0 when the pump is blocked, so $\Delta R/R_0$ and $\Delta T/T_0$. In what follows we will refer to $\Delta R/R_0$ as the reflection change and to $\Delta T/T_0$ as the transmission change.

The samples used in the experiments are prepared using physical vapor deposition at a pressure below 10^{-6} mbar. The substrates are chemically cleaned glass plates with a thickness of 2 mm. During the evaporation process, the deposited film thickness was monitored using a quartz crystal oscillator. Scanning Electron Microscope (SEM) images of all samples were made before and after the experiments were performed. An example image of an undamaged sample with an effective film thickness of 6 nm is shown in the inset of Fig. 1. All samples show a similarly nanostructured Au layer, typical for Au deposited on glass with an effective thickness at, or close to, the percolation threshold. We find the effective fraction of the surface covered in Au to be 0.85, which is somewhat above the reported percolation threshold of 0.68 [11]. All gold layers have an average thickness of 6 nm and SEM images show that all gold layers have a similar percolating morphology.

To determine whether laser-substrate interaction plays a role in our experiments, pump-probe measurements were also performed on the bare substrate for all pump energies. No transient effect was measured on a timescale of our experiments on a timescale of 0 to 1 ns, except for a small, pulse duration limited instantaneous effect at t=0. This we attribute to the coherent coupling between the pump and probe beam in the substrate. This coherent coupling gives rise to apparent changes in probe reflectivity and transmission, which were measured to be less than 1% for our highest used pump energy. Furthermore, optical microscopy images of the substrate after the experiment show no permanent alteration of the substrate.

Optics EXPRESS

3. Results

In this section we will describe the measured results, both the time-dependent transmission and reflection changes, and the aftermath. In section 4 the results will be discussed in further detail and an interpretation of the results will be given.

3.1. Power dependence

In Figs. 2(a) and 2(b) we plot the time-dependent pump-induced reflection and transmission change during the first 15 ps after excitation of a percolating gold layer, for ten different values of the pulse energy, ranging from 1 μJ to 100 μJ. These pulse energies correspond to a fluence range of 0.0127 J/cm^2 to 1.27 J/cm^2 and an intensity range of 2.3×10^{11} W/cm^2 to 2.3×10^{13} W/cm^2. We define the intensity here as the pulse energy divided by the pulse duration divided by beam surface area determined by the FWHM diameter of the beam on the sample.

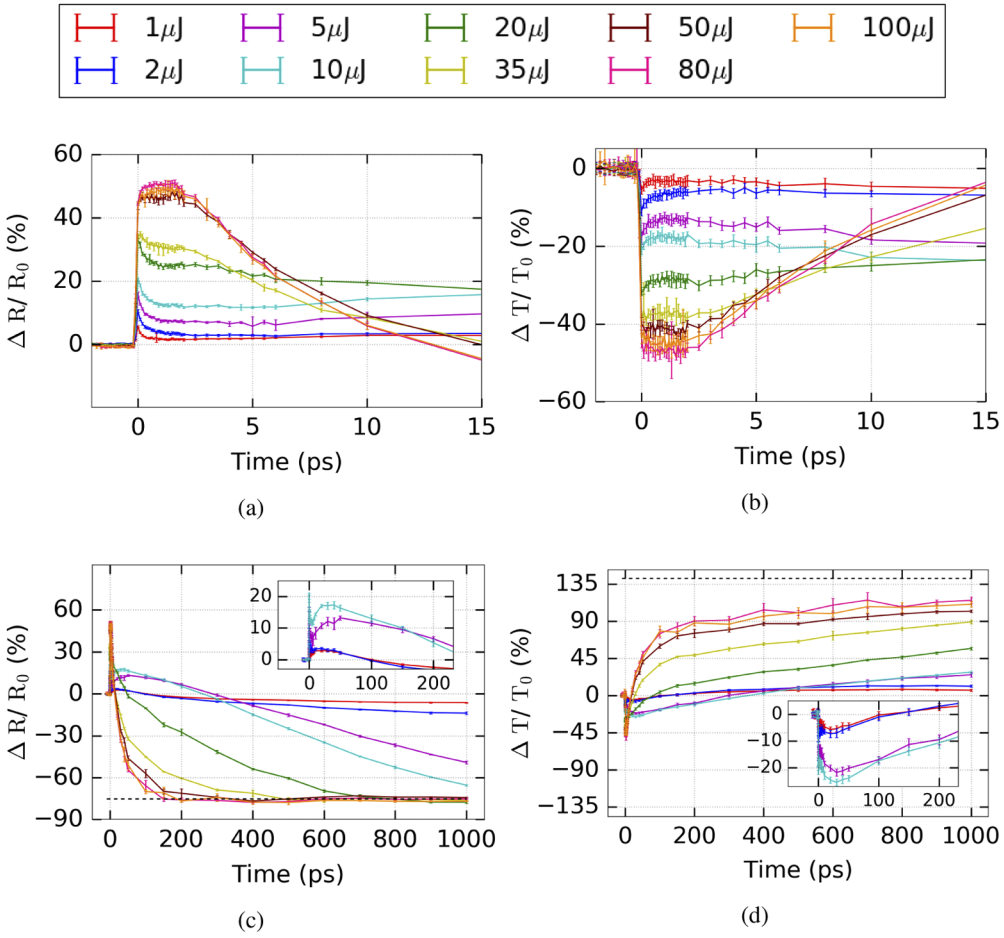

Fig. 2. (a), (c) Pump-induced reflection change and, (b), (d) transmission change as a function of delay between the pump and probe pulses for pump pulse energies ranging from 1 to 100 μJ and on two different time scales. At t=0 ps the pump and probe overlap in time. Both the pump and the probe have a wavelength of 1.3 μm.

For all pump energies, when pump and probe overlap in time at t=0, we observe a pulse length limited increase in the reflection change $\Delta R/R_0$ and a pulse length limited decrease in

Optics EXPRESS

the transmission change $\Delta T/T_0$. Both become larger with increasing pump fluence. For pump energies of 35 μJ and less, we measure a small quasi-exponential decrease in reflection change in the first two picoseconds. For pulse energies of 1, 2, 5, and 10 μJ this is followed by a slow increase on a 15 ps time scale, whereas for the pulse energies of 20 and 35 μJ this is followed by a signal decrease. For pump pulse energies of 50 μJ and higher, the reflection changes reach values of approximately 50% and vary little during the first two picoseconds. After two picoseconds, the signals begin to decay and become negative. Very similar effects are seen for measurements of the transmission change, which are opposite in sign compared to the reflection change.

In Figs. 2(c) and 2(d) we plot the time-dependent pump-induced reflection and transmission changes of the percolating Au samples for time delays up to one nanosecond. We show that for pump energies of 10 μJ and lower the slow increase of the reflection change, seen in Fig. 2(a) after two picoseconds, continues for a few tens of picoseconds [inset of Fig. 2(c)]. Afterward, a decrease to negative values occurs on a time scale of hundreds of picoseconds. Again, similar effects can be seen for the transmission measurements, but with opposite sign. For pulse energies of 20 μJ and higher, after staying relatively constant during the first two picoseconds, the reflection change drops, becomes negative and reaches a value that corresponds to an absolute reflection of about 9% ($\Delta R/R = -75\%$), indicated by the black dashed line. This value of 9% corresponds to the absolute reflectivity measured on a bare substrate under the same experimental conditions [15]. The rate of the decrease in the reflection change for these high fluences grows with increasing pulse energy.

3.2. SEM analysis

So far, we have described the ultrafast pump-induced changes in the reflection and transmission of the percolating gold layers on a time scale of up to 1 ns. In this section we will show SEM images taken of the samples before and after illumination for different pulse energies.

In Figs. 3(a) and 3(b) we show the SEM images for two different magnifications of the sample surface after illumination with a pump pulse with an energy of 1 μJ on two different length scales. In Fig. 3(c) we show the location of the SEM images on an optical microscopy image of the entire crater. Note that on the microscopy image the crater looks black, indicating no material present. However, closer inspection using the SEM shows that this is not the case. We notice that, in contrast with images made for higher pump energies, the gold in the center has not been fully removed but now shows larger holes whilst in between these holes the percolating Au structure is still in pristine condition. The structure of the center of the illuminated regime closely resembles that of the edge of the craters for higher pump energies, as becomes clear when comparing Fig. 3(b) with Fig. 4(b), where we show the crater edge for a pulse energy of 35 μJ. We note that in the case of illumination with a 1 μJ pulse, ablation only occurs locally. Therefore, we can determine the ablation threshold by calculating the intensity for a 1 μJ pump pulse. Thus, we find that the intensity at which removal of the gold starts taking place, equals 2.3×10^{11} W/cm^2. The ablation threshold we measured is on the same order of magnitude as the ablation threshold measured for trapped single spherical gold nanoparticles [16].

In Figs. 4(a) and 4(b), we show typical SEM images of the sample surface both before and after illumination, respectively, with a pump pulse energy of 35 μJ. The image of the aftermath is taken at the left edge of the pump-induced crater, as indicated by the arrow in Fig. 4(c). For all pulse energies above 5μJ used in the experiment similar images were obtained but not shown. In the experiment, the transverse beam profile of the pump resembles a Gaussian, with a beam diameter of approximately 100 μm. Due to the Gaussian-like shape of the pulse a transverse pump intensity gradient is present on the Au surface. As a result, in Fig. 4(b) we observe a transition from little damage on the left side of the image to significant damage on the right side, which is closer to the center of the beam. In Fig. 4(b) the crater begins when moving further to the right. Furthermore, we note that the gold layer is curling up at the edges of the crater.

Optics EXPRESS

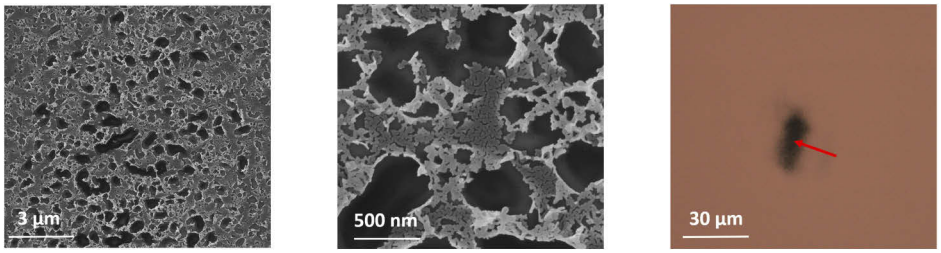

(a) (b) (c)

Fig. 3. (a) SEM image of the sample illuminated with a 1 μJ pump pulse. (b) Zoomed-in image of the sample. At these pump intensities, the gold layer is damaged but has not been fully removed in the center. Note that large holes have appeared in the layer and that the edges of the holes curl over. In between the large holes the original percolating structure of the Au is still present, indicating that the intensity used here is close to the ablation threshold. (c) Optical microscopy image of the crater. The red arrow gives an indication of the location where the SEM images were taken.

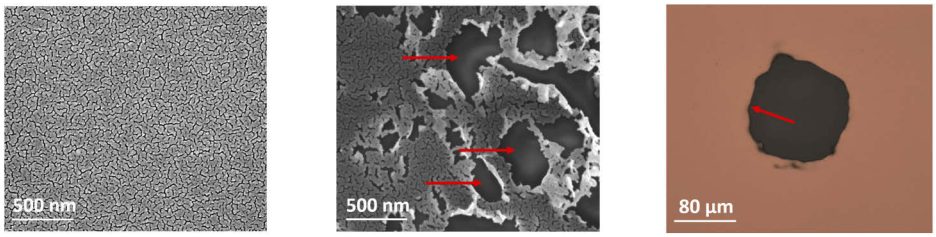

(a) (b) (c)

Fig. 4. SEM images of the percolating Au surface, before (a) and after (b) illumination with a 35μJ single laser pulse. In (b) we show the left edge of the pump-induced crater. We observe local removal of gold from the surface. The red arrows indicate regions where the gold has been removed and the substrate is visible. Furthermore, at the edge of the holes the gold is curling over indicating violent removal of the gold. (c) Optical microscopy image of the crater. The red arrow gives an indication of the location where the SEM image of (b) was taken.

In Figs. 5(a) and (b) we show more detailed SEM images of the edge of the crater at two different magnifications for a sample illuminated with a pump energy of 100 μJ. Here it can be clearly seen that the gold at the edge has become detached from the substrate and is curling up, indicating violent removal of material. Furthermore, next to the crater edge there is a small band where no gold is present, which is the location where the curled-over gold used to be. Due to the rapid heating of the lattice and vaporization, a pressure will develop at the substrate-film interface and at the free surface. The curling over of the gold indicates that the pressure developed at the substrate film interface exceeds that of the pressure developed on the free surface, causing the gold to violently detach.

Further towards the center of the crater is a region where isolated nano-islands of gold are present with a diameter of approximately 50 nm. This region extends 20 μm towards the center of the crater. Optical microscopy and SEM analysis show that there is no more gold left in the crater center itself. Due to charging effects of the substrate during SEM, clear imaging of the center of the crater was not possible.

Optics EXPRESS

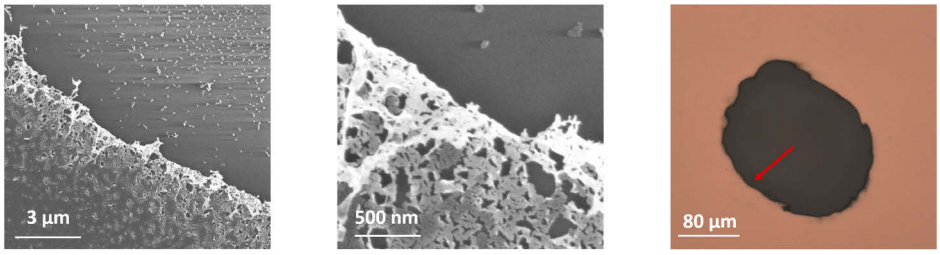

(a) (b) (c)

Fig. 5. (a) SEM image of the crater edge. The sample was illuminated with a pulse energy of 100 μJ. The transition of the non-damaged percolating Au (bottom left) to a damaged region closer to the crater center (top right) can be seen. In the top right half of the figure many nano-islands of gold are visible. These isolated nano-islands of gold are present for the first 20 μm, starting from the crater edge towards the crater center, except in the region where the curled-over gold used to be. In between the nano-islands the bare substrate (darker grey) can clearly be seen. (b) Zoomed-in SEM image of the crater edge, Note the different length scales indicated in the figures. (c) Shows an optical microscopy image of the crater. The red arrow gives an indication of the location where the SEM images were taken.

4. Discussion

The interaction between ultrafast laser pulses and various materials has been investigated extensively in the past [14,17–22]. When a femtosecond laser pulse irradiates a metal, the energy is partly absorbed by the electrons, creating a non-thermal electron distribution [23,24]. The electron gas then thermalizes into a Fermi-Dirac distribution on a timescale of several hundreds of femtoseconds [25,26]. This so-called thermalization time has been shown to decrease with increasing laser power [26]. During and after thermalization, energy is exchanged with the lattice via electron-phonon coupling [27–29]. The timescale of electron energy transfer to the lattice is governed by the electron-phonon coupling constant g, which is unique for every metal [30].

This process of energy exchange between the electrons and the lattice can be described by the two-temperature model (TTM), as first proposed by Anisimov et al. [31]. This model consists of two coupled differential equations describing the temporal and spatial evolution of both the electron temperature T_e and the lattice temperature T_l. Both the electron gas and the lattice have their own heat capacities, C_e and C_l, respectively. The heat capacities themselves can also exhibit a temperature dependency at high temperatures. In general, the electron heat capacity is much smaller than the lattice heat capacity, allowing the electrons to heat up to relatively high temperatures, even for low fluences.

It has been shown that the process of energy transfer to the lattice occurs on a timescale of 1-10 ps for Au [32–34]. An estimate of the theoretical lattice temperature attained in our experiment can be made by taking the pump pulse energy absorbed in a disk of percolating gold with an effective thickness of 6 nm and a diameter equal to the diameter of the pump beam. It has been shown that for thin gold layers with a thickness of $\approx$ 50 nm the heat capacity is not different with respect to the bulk lattice heat capacity [35]. However, the heat capacity for a 6 nm thick percolating layer might be different, but the exact value is not known to us. Therefore, as a *rough* approximation, in our calculations we use the lattice heat capacity of a 50 nm thick gold layer at room temperature, having a value of 2.44×10^6 Jm^{-3}K^{-1}. Furthermore, assuming an incident pulse energy of 100 μJ, a *measured* absorptivity of 0.32 and a beam diameter of about 100 μm, we calculate a lattice temperature of 2.78×10^5 K. This temperature of course well exceeds the melting and boiling temperature for Au (1338 K and 3243 K respectively) and is therefore not the real temperature reached. It does indicate, however, that extreme conditions are reached in our

Optics EXPRESS

experiments. One of the reasons for this is the structure of the percolating surface. The percolating Au absorptance (A_p) is higher for 1300 nm light than the absorptance of a flat continuous Au layer (A_c). We found in our experiments that $A_p \approx 16A_c$. It is known that percolating gold absorbs considerably more light than continuous layers of gold and therefore heats up more. The increased absorption is typically attributed to the excitation of localized plasmons in the nano-structured material [36,37]. In turn, this can lead to local field enhancements which can lower the average damage threshold for percolating gold compared to that for continuous layers of gold.

In what follows we will provide a qualitative explanation for the reflection and transmission changes observed on different timescales.

4.1. 0 - 0.5 ps, electron excitation

For both the reflection and transmission change, as seen in Figs. 2(a) and 2(b) respectively, we measure a pulse length limited increase in reflection and a decrease in transmission around t=0 ps, corresponding to an increase in absorption. Due to the strong excitation by the pump pulse the electron distribution, as described by a Fermi-Dirac distribution, starts to smear out. This smearing of the electron distributions results in a reduction of the electronic occupancy below the Fermi energy as sketched by the dashed area in Fig. 6. In this figure we show the electronic density of states (DOS) of the d-band together with the electron distribution of the hybridized s/p-band as a mere schematic representation of the new pump-induced allowed interband transitions with energy $E(\omega)$. It has been shown that such a reduction of electronic occupancy below the Fermi energy can lead to an increase in absorption [17], as lower energy photons can now induce optical transitions from the shallow d-band to the hybridized s/p-band [38,39]. Thus it may become feasible for our probe photons with a relatively low energy $E(\omega)$ (Fig. 6) to excite previously forbidden *interband* transitions, consequently increasing the absorption. In general, we also

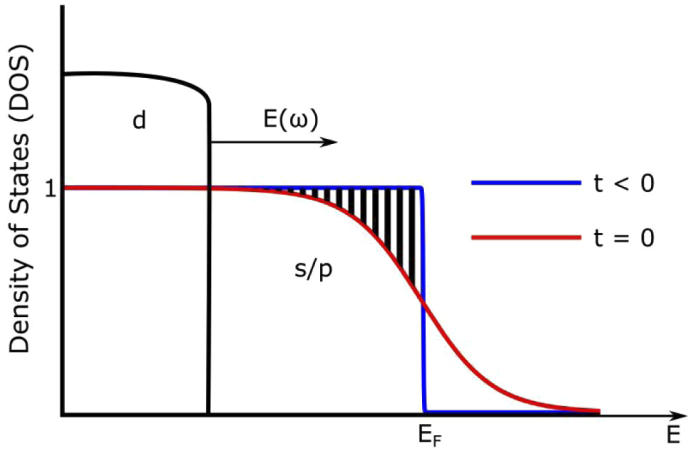

Fig. 6. Schematic depiction of the broadening of the electronic occupation distribution and the consequently induced availability of intraband transitions from the d-band. Here we show the DOS of the d-band together with the Fermi distribution of the electrons of the hybridized s/p-band as a schematic representation of the possibility to excite electrons from the d- to the s/p-band. See [38] for a more accurate depiction of the actual DOS of the d-band of Au. In blue we show the unperturbed electron distribution, in red we show the electron distribution as changed by the pump pulse. The probe photon energy $E(\omega)$ is represented by the black arrow. Due to broadening of the electron distribution, optical interband transitions for probe photons with an energy of $E(\omega)$ become possible.

Optics EXPRESS

induce *intraband* transitions, which have been shown to increase the reflectivity in Au as well [40].

In Figs. 7(a) and 7(b) we plot the reflection and transmission change at t=0 ps versus pump pulse energy. We see that the magnitude of the reflection and transmission change saturates for higher pump energies. For the reflection and transmission change, saturation occurs for pulse energies on the order of 50 μJ at a value of ~50% for the reflection change and at a value ~-45% for the transmission change.

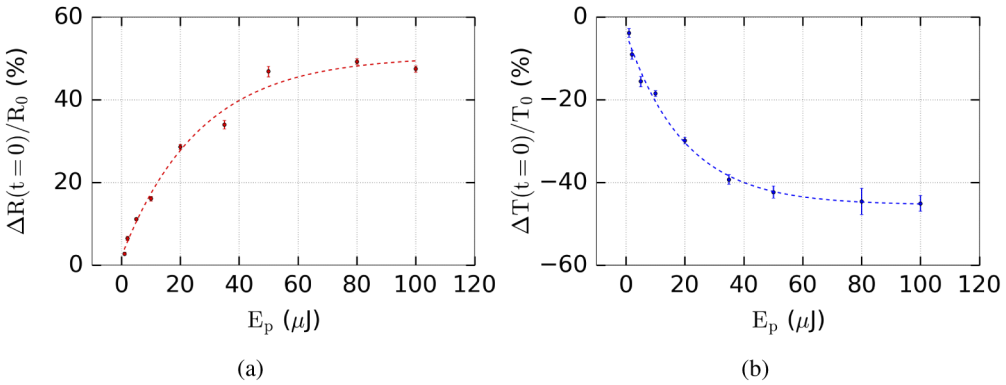

Fig. 7. Pump-induced reflection change (a) and transmission change (b) at t=0 ps as a function of the pump pulse energy. The dashed line is an exponential fit and should be considered a guide to the eye.

We note that the reflection and transmission change start to saturate for high pump energies. We speculate that this is because the *changes* in electronic occupancy start to saturate due to the saturation of the broadening of the Fermi-distribution which begins to flatten out at high pump energies. For high electron temperatures the change in the smeared-out electron distribution becomes less significant for further temperature increases and thus, changes in the optical response saturate as well. Saturation of the reflectivity change as a function of incident pump energy has been shown before for continuous gold [18] but, to our knowledge, not for percolating gold and never simultaneously in transmission and reflection and not for the intensities used in our experiments, which are at least two orders of magnitude above the damage threshold. Note, however, that the physics is likely to be complicated by the high probability that at these intensities, energetic electrons are capable of promoting electrons from the d-band to the s/p-band, thus increasing the number of carriers in the s/p-band.

4.2. 0.5 - 30 ps, lattice relaxation

For pump pulse energies below 50 μJ we observe a quasi-exponential decrease in the reflection change and an increase in the transmission change in the first 2 ps after excitation.

When the metal layer is thin, the electron gas inside the layer homogeneously heats up. Under these circumstances, electron energy diffusion can be neglected and it was shown that this causes the electron gas temperature to decay linearly with time [14,24]. However, the observed exponential decay seems to indicate that this does not play a role here. It has also been suggested that for noble metals a non-thermalized electron gas experiences a stronger electron-phonon coupling than a thermalized electron gas [24]. This implies that when the electron gas thermalizes and the coupling with the lattice decreases, the energy transfer rate to the lattice slows down. However, as mentioned in the beginning of section 4, we expect the thermalization time to increase with laser power and to be significantly shorter than 2 ps [41].

Optics EXPRESS

Instead, we think that the temperature-dependent electron-phonon coupling strength is responsible for the observed quasi-exponential decay. At lower power it has been shown that in Au the electron gas will cool by heating the lattice on a timescale of 10-15ps [42]. However, for high electron temperatures, the electron-phonon coupling constant exhibits a temperature dependence [43]. At electron temperatures of about 2000 K and higher the electron-phonon coupling constant g increases and becomes proportional to T_e and T_l, i.e. $g \propto T_e + T_l$. It was shown that g can increase by as much as a factor of 6 when reaching electron temperatures on the order of 2×10^4K [38,44], which is very likely in our experiments.

Assuming a linear relationship between the electron heat capacity and the electron temperature, i.e. $C_e(T_e) \propto T_e$ [45], which is normally only valid for electron temperatures below 2000 K, we can calculate as a rough estimate that the electron temperature reached under our experimental conditions for the highest used pump energy of 100 μJ equals $\approx 1.5 \times 10^5$ K. This is of course a gross overestimate of the actual electron temperature due to the non-linear behavior of the electronic heat capacity at high temperatures. However, it gives an upper limit on the electron temperature and shows that under our experimental conditions, we can no longer assume that the electron-phonon coupling constant g is independent of the electron temperature. An increase of g will in turn increase the initial rate at which energy is transferred from the electron gas to the lattice, explaining the observation of an initial fast signal decay in our experiment.

We speculate that after 2 ps the electrons have cooled off substantially, lowering the electron-phonon coupling constant and decreasing the energy exchange rate, slowing down the cooling of the electron gas. Simultaneously, the lattice is heating up, increasing the reflection and decreasing the transmission at a timescale of approximately 30 ps, as can be seen in the insets of Figs. 2(c) and 2(d). These two competing effects of the electron-cooling and lattice-heating can explain the shape of the curves of the optical response on a timescale of 0.5 - 30 ps.

For pump pulse energies of 50 μJ and higher we measure a constant plateau in both the reflection- and transmission change in the first 2 ps. When the electron gas transfers its energy to the lattice the electron distribution will relax to its original shape. However, since the change of the electron distribution is "saturated" it takes time for this relaxation to affect the optical parameters, thus creating a plateau. Simultaneously the lattice will heat up to extreme temperatures resulting in the rapid heating, melting and, possibly, vaporization of the lattice. We speculate that at pulse energies above 10 μJ the morphological changes to the lattice occur before non-destructive changes in the lattice temperature have had the time to affect the reflection and the transmission. Therefore, the "bulge" in reflection and transmission as seen for pulse energies below 10 μJ in the insets of Figs. 2(c) and 2(d) is absent for pulse energies above 10 μJ. This rapid heating, melting and, possibly, vaporization of the Au results in a steep decrease in reflection and an increase in transmission.

4.3. 30 - 1000 ps, vaporization

On longer timescales we see that the transmission values start to increase dramatically whilst the reflection values start to decrease and are even approaching the substrate values. This combined behavior of both reflection and transmission is strong evidence that the Au layer is becoming optically transparent on a remarkably short timescale of about 150 ps. This suggests that the excited layer has in fact vaporized into a mist of atoms and small particles, distributed over a larger volume in a direction predominantly perpendicular to the surface. It has been shown that this process of vaporization is possible via dissociation of the entire layer when the injected energy exceeds the cohesive energy of the material [46,47]. Using the pump pulse energy and beam size we can calculate the absorbed energy per gold atom. For 100 μJ pulse energy we calculate that the absorbed energy equals 59 eV/atom, whilst the cohesive energy of gold equals 3.81 eV/atom [45]. For all pulse energies above 5 μJ the absorbed energy per atom exceeds the cohesive energy of gold. For lower pulse energies the average absorbed energy per atom is lower

Optics EXPRESS

than the cohesive energy. However, near-field optical hotspots due to the percolating nature of our film can lead to an enhanced absorbed energy which locally exceeds the cohesive energy. Therefore, locally the threshold for removal of material is reached whereas it is not reached at other locations, explaining the morphology seen for the lowest fluences, see Fig. 3(b). It is important to realize that this process of vaporization is not the traditional vaporization process characterized by the Hertz-Knudsen equation which describes only vaporization from the outer surface. Hertz-Knudsen surface vaporization happens on timescales larger than 1 ns and is thus too slow to explain our experimental data [48].

The maximum reflection change possible in our system is when the absolute reflection equals the substrate reflection, which corresponds to a reflection change of ≈ -75%. When the reflection change reaches this value, the density of the mist of atoms/particles has decreased in such a manner that it has become nearly fully optically transparent for our probe pulse. We use only the reflection here because, although the transmission dramatically increases for the highest intensities, it has not yet fully reached the value of the bare substrate-level. We suspect that this is caused by thermal lensing effects present in the substrate, which could diffract/refract some light away from the detector. However, more research is needed to confirm this hypothesis.

From our reflection measurements, we can derive the time τ_{tr} it takes for the Au gold to become optically transparent. The experimental data starting from Fig. 2(c) was fitted to an exponential function starting at 50 ps decaying to an asymptote of -75%, which corresponds to an absolute reflection close to that of the substrate. The time τ_{tr} is somewhat arbitrarily chosen as the time it takes for the reflection change to drop below -70%. For the pulse energies below 20 μJ extrapolation of the fit was necessary to retrieve τ_{tr}. For pulse energies below 10 μJ the τ_{tr} was not extracted as the uncertainty in the extrapolated values for was too large for these slowly changing curves.

In Fig. 8, we show τ_{tr} as a function of the pulse energy. The dashed line is an exponential fit to the data which acts as a guide to the eye. We can see that for pulse energies larger than about 50 μJ, the sample reaches the substrate reflection levels, indicating that the percolating gold layer has transformed into a mist of atoms and/or small particles and has become optically transparent within approximately 150 ps.

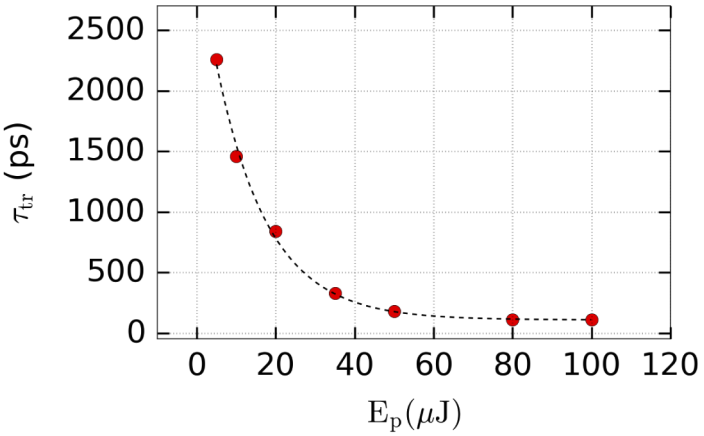

Fig. 8. Time τ_{tr} before sample becomes transparent as a function of pump pulse energy. The dashed line is a decaying exponential and should be considered a guide to the eye.

In Figs. 9(a) and 9(b) we show the reflection and transmission change respectively as a function of pulse energy at t = 1 ns. Note how the reflection has reached the substrate value at this point for all pulse energies of 20 μJ and higher. We see that for the pulses with 10 and 20 μJ the substrate level has not yet been reached, indicating that the mist of atoms/particles is still partially

Optics EXPRESS

opaque. The transmission change shows similar saturation-like dynamics, but possibly due to the thermal lensing effect discussed previously, it has not completely saturated.

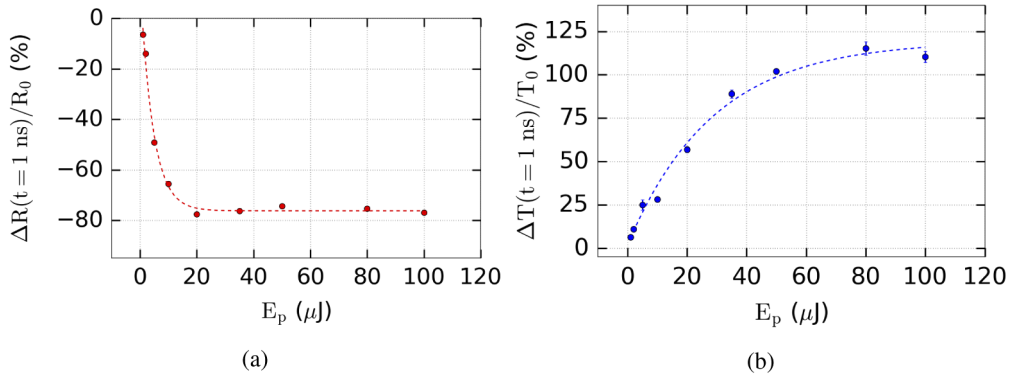

Fig. 9. Pump-induced reflection change (a) and transmission change (b) at t=1 ns as a function of the pump pulse energy. The dashed line is an exponential fit and should be considered a guide to the eye.

In Fig. 10 we show the final diameter of the crater versus the incident pulse energy. The crater diameter was determined by measuring the surface area of the ablated crater and calculating an effective diameter corresponding to a circle with the same surface area. Note that for the pulse energies of 1 and 2 μJ, the resulting crater diameter is smaller than the $1/e^2$ size of the probe. This explains why we do not see the reflection and transmission values approach the substrate value, as can be seen in Figs. 9(a) and 9(b). For these pulse energies, a part of the probe beam still illuminates gold which has not been ablated. Due to this, the observed response in the measurements is not solely caused by ablation dynamics. Rather, it is a combination of measurements of the ablation effects in the part of the probe beam overlapping with, what will

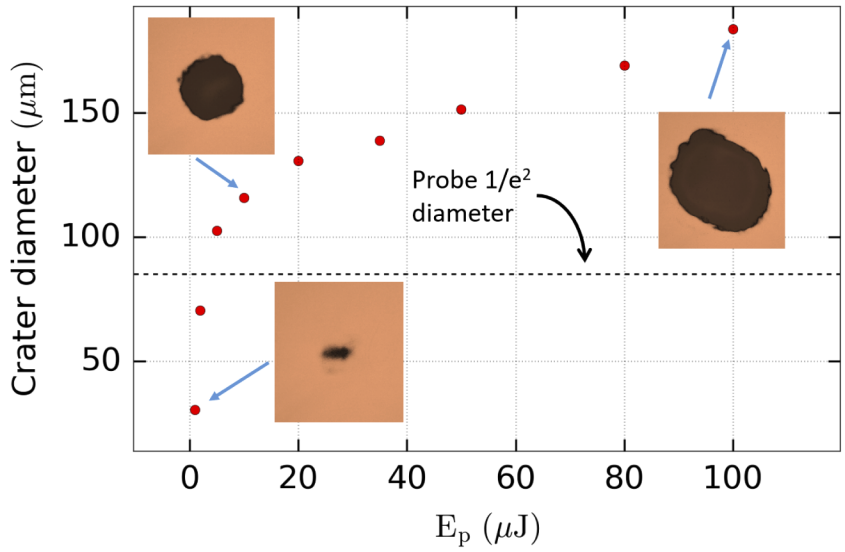

Fig. 10. Crater diameter versus the pump pulse energy. The black dashed line represents the $1/e^2$ diameter of the probe. The three insets are optical microscopy images of the final crater.

Optics EXPRESS

later become the crater and of non-destructive excitation in the part of the probe beam that does not overlap with the crater area.

5. Conclusion

We have shown transient pump-probe reflection and transmission measurements on percolating gold layers on glass substrates in the ablation regime. Our measurements show a strong increase in reflection and a decrease in transmission directly after optical excitation. This is attributed to the increasing electron temperature and the subsequent Fermi-smearing of the electron distribution, resulting in a reduction of the electronic occupancy. Fermi smearing of the electron distribution enables excitations from the d-band to the hybridized s/p-band, increasing the absorption.

On longer times scales and for the highest intensities, both the reflection and transmission approach the values of the substrate on a timescale of about 150 ps, indicating that the Au layer becomes optically transparent. We argue that the vaporization of the entire layer into a mist of atoms and small particles is the most plausible explanation for this behavior. This process of vaporization is possible because the absorbed energy exceeds the cohesive energy of the gold atoms. We find that the ablation threshold of percolating gold layers is some two orders of magnitude lower than the values found for continuous layers of gold in the literature.

Funding

Nederlandse Organisatie voor Wetenschappelijk Onderzoek; Universiteit van Amsterdam; ASML.

Acknowledgments

This work was conducted at the Advanced Research Center for Nanolithography, a public-private partnership between the University of Amsterdam, Vrije Universiteit Amsterdam, the Netherlands Organization for Scientific Research (NWO), and the semiconductor-equipment manufacturer ASML. The authors declare no conflicts of interest.

Disclosures

The authors declare no conflicts of interest.

References

1. H. Gleiter, "Nanostructured materials: basic concepts and microstructure," Acta Mater. **48**(1), 1–29 (2000).
2. D. Stauffer and A. Aharony, "Introduction to Percolation Theory," (CRC press, 1994) 2nd ed.
3. D. I. Yakubovsky, Y. V. Stebunov, R. V. Kirtaev, G. A. Ermolaev, M. S. Mironov, S. M. Novikov, A. V. Arsenin, and V. S. Volkov, "Ultrathin and Ultrasmooth Gold Films on Monolayer MoS2," Adv. Mater. Interfaces **6**, 1900196 (2019).
4. G. K. Ramanandan, G. Ramakrishnan, N. Kumar, A. J. Adam, and P. C. M. Planken, "Emission of terahertz pulses from nanostructured metal surfaces," J. Phys. D: Appl. Phys. **47**(37), 374003 (2014).
5. G. Ramakrishnan and P. C. M. Planken, "Percolation-enhanced generation of terahertz pulses by optical rectification on ultrathin gold films," Opt. Lett. **36**(13), 2572 (2011).
6. D. K. Polyushkin, E. Hendry, and W. L. Barnes, "Controlling the generation of THz radiation from metallic films using periodic microstructure," Appl. Phys. B **120**(1), 53–59 (2015).
7. M. Breit, G. Von Plessen, J. Feldmann, S. Grésillon, J. C. Rivoal, P. Gadenne, V. A. Podolskiy, A. K. Sarychev, and V. M. Shalaev, "Experimental observation of percolation-enhanced nonlinear light scattering from semicontinuous metal films," Phys. Rev. B **64**(12), 125106 (2001).
8. V. M. Shalaev and A. K. Sarychev, "Nonlinear optics of random metal-dielectric films," Phys. Rev. B **57**(20), 13265–13288 (1998).
9. P. Gadenne, Y. Yagil, and G. Deutscher, "Transmittance and reflectance in situ measurements of semicontinuous gold films during deposition," J. Appl. Phys. **66**(7), 3019–3025 (1989).
10. Y. Yagil, P. Gadenne, C. Julien, and G. Deutscher, "Optical properties of thin semicontinuous gold films over a wavelength range of 2.5 to 500 μm," Phys. Rev. B **46**(4), 2503–2511 (1992).
11. M. Walther, D. G. Cooke, C. Sherstan, M. Hajar, M. R. Freeman, and F. A. Hegmann, "Terahertz conductivity of thin gold films at the metal-insulator percolation transition," Phys. Rev. B **76**(12), 125408 (2007).

Optics EXPRESS

12. G. Dumpich, S. Friedrichowski, and P. Mikitisin, "Electron transport in percolating gold films," Thin Solid Films **281-282**, 368–371 (1996).
13. G. T. Boyd, T. Rasing, J. R. R. Leite, and Y. R. Shen, "Local-field enhancement on rough surfaces of metals, semimetals, and semiconductors with the use of optical second-harmonic generation," Phys. Rev. B **30**(2), 519–526 (1984).
14. J. Hohlfeld, S.-S. Wellershoff, J. Güdde, U. Conrad, V. Jähnke, and E. Matthias, "Electron and lattice dynamics following optical excitation of metals," Chem. Phys. **251**(1-3), 237–258 (2000).
15. This is the sum of the reflections of the front and back surfaces of the substrate.
16. J. Hernandez-Rueda, A. de Beurs, and D. van Oosten, "Ultrafast laser ablation of trapped gold nanoparticles," Opt. Lett. **44**(13), 3294 (2019).
17. J. Hohlfeld, D. Grosenick, U. Conrad, and E. Matthias, "Femtosecond time-resolved reflection second-harmonic generation on polycrystalline copper," Appl. Phys. A **60**(2), 137–142 (1995).
18. J. Hohlfeld, U. Conrad, J. G. Müller, S.-S. Wellershoff, E. Matthias, and K. H. Bennemann, "Nonlinear Optics in Metals," (Oxford University, 1998), pp. 219–267.
19. J. Hernandez-Rueda, J. Clarijs, D. Van Oosten, and D. M. Krol, "The influence of femtosecond laser wavelength on waveguide fabrication inside fused silica," Appl. Phys. Lett. **110**(16), 161109 (2017).
20. J. Hernandez-Rueda and D. van Oosten, "Transient scattering effects and electron plasma dynamics during ultrafast laser ablation of water," Opt. Lett. **44**(7), 1856 (2019).
21. M. Vreugdenhil, D. van Oosten, and J. Hernandez-Rueda, "Dynamics of femtosecond laser-induced shockwaves at a water/air interface using multiple excitation beams," Opt. Lett. **43**(20), 4899 (2018).
22. D. Von Der Linde and K. Sokolowski-Tinten, "Physical mechanisms of short-pulse laser ablation," Appl. Surf. Sci. **154-155**, 1–10 (2000).
23. R. H. M. Groeneveld, R. Sprik, and A. Lagendijk, "Femtosecond spectroscopy of electron-electron and alectron-phonon energy relaxation in Ag aund Au," Phys. Rev. B **51**(17), 11433–11445 (1995).
24. B. Rethfeld, D. S. Ivanov, M. E. Garcia, and S. I. Anisimov, "Modelling ultrafast laser ablation," J. Phys. D: Appl. Phys. **50**(19), 193001 (2017).
25. C.-K. Sun, F. Vallée, L. H. Acioli, E. P. Ippen, and J. G. Fujimoto, "Femtosecond-tunable measurement of electron thermalization in gold," Phys. Rev. B **50**(20), 15337–15348 (1994).
26. B. Y. Mueller and B. Rethfeld, "Relaxation dynamics in laser-excited metals under nonequilibrium conditions," Phys. Rev. B **87**(3), 035139 (2013).
27. L. Jiang and H.-L. Tsai, "Improved Two-Temperature Model and Its Application in Ultrashort Laser Heating of Metal Films," J. Heat Transfer **127**(10), 1167–1173 (2005).
28. M. Kaganov, E. Lifshitz, and L. Tanatarov, "Relaxation between electrons and the crystalline lattice," Sov. Phys. Jetp-Ussr **4**, 173–178 (1957).
29. J. Hohlfeld, J. G. Müller, S. S. Wellershoff, and E. Matthias, "Time-resolved thermoreflectivity of thin gold films and its dependence on film thickness," Appl. Phys. B **64**(3), 387–390 (1997).
30. S. D. Brorson, A. Kazeroonian, J. S. Moodera, D. W. Face, T. K. Cheng, E. P. Ippen, M. S. Dresselhaus, and G. Dresselhaus, "Femtosecond room-temperature measurement of the electron-phonon coupling constant in metallic superconductors," Phys. Rev. Lett. **64**(18), 2172–2175 (1990).
31. S. I. Anisimov and B. L. Kapeliovich, "Electron emission from metal surfaces exposed to ultrashort laser pulses," J. Exp. Theor. Phys. **39**, 375–377 (1974).
32. B. N. Chichkov, C. Momma, S. Nolte, F. Von Alvensleben, and A. Tünnermann, "Femtosecond, picosecond and nanosecond laser ablation of solids," Appl. Phys. A **63**(2), 109–115 (1996).
33. R. W. Schoenlein, W. Z. Lin, J. G. Fujimoto, and G. L. Eesley, "Femtosecond studies of nonequilibrium electronic processes in metals," Phys. Rev. Lett. **58**(16), 1680–1683 (1987).
34. X. Y. Wang, D. M. Riffe, Y.-S. Lee, and M. C. Downer, "Time-resolved electron-temperature measurement in a highly excited gold target using femtosecond thermionic emission," Phys. Rev. B **50**(11), 8016–8019 (1994).
35. D. R. Queen and F. Hellman, "Thin film nanocalorimeter for heat capacity measurements of 30 nm films," Rev. Sci. Instrum. **80**(6), 063901 (2009).
36. V. M. Shalaev, "Nonlinear Optics of Random Media," (Springer, 2000).
37. V. M. Shalaev, "Optical Properties of Nanostructured Random Media," (Springer, 2002).
38. Z. Lin, L. V. Zhigilei, and V. Celli, "Electron-phonon coupling and electron heat capacity of metals under conditions of strong electron-phonon nonequilibrium," Phys. Rev. B **77**(7), 075133 (2008).
39. C. Fourment, F. Deneuville, D. Descamps, F. Dorchies, S. Petit, O. Peyrusse, B. Holst, and V. Recoules, "Experimental determination of temperature-dependent electron-electron collision frequency in isochorically heated warm dense gold," Phys. Rev. B **89**(16), 161110 (2014).
40. A. N. Smith and P. M. Norris, "Influence of intraband transitions on the electron thermoreflectance response of metals," Appl. Phys. Lett. **78**(9), 1240–1242 (2001).
41. B. Rethfeld, V. V. Temnov, K. Sokolowski-Tinten, P. Tsu, D. von der Linde, S. I. Anisimov, S. I. Ashitkov, and M. B. Agranat, "Superfast thermal melting of solids under the action of femtosecond laser pulses," J. Opt. Technol. **71**(6), 348 (2004).

Optics EXPRESS

42. S. Edward, A. Antoncecchi, H. Zhang, H. Sielcken, S. Witte, and P. C. M. Planken, "Detection of periodic structures through opaque metal layers by optical measurements of ultrafast electron dynamics," Opt. Express **26**(18), 23380–23396 (2018).
43. J. K. Chen, W. P. Latham, and J. E. Beraun, "The role of electron-phonon coupling in ultrafast laser heating," J. Laser Appl. **17**(1), 63–68 (2005).
44. J. Yang, Y. Zhao, and X. Zhu, "Theoretical studies of ultrafast ablation of metal targets dominated by phase explosion," Appl. Phys. A **89**(2), 571–578 (2007).
45. C. Kittel, "Introduction to Solid State Physics," (John Wiley & Sons, 1986), 6th ed.
46. D. Perez and L. J. Lewis, "Molecular-dynamics study of ablation of solids under femtosecond laser pulses," Phys. Rev. B **67**(18), 184102 (2003).
47. P. Lorazo, L. J. Lewis, and M. Meunier, "Thermodynamic pathways to melting, ablation, and solidification in absorbing solids under pulsed laser irradiation," Phys. Rev. B **73**(13), 134108 (2006).
48. A. Miotello and R. Kelly, "Laser-induced phase explosion: New physical problems when a condensed phase approaches the thermodynamic critical temperature," Appl. Phys. A **69**(7), S67–S73 (1999).